Sulfonic acid functionalized magnetite nanomesoporous carbons for removal of Safranin O from aqueous solutions

Sanaz Toutounchi[a], Shahab Shariati[b,*], Kazem Mahanpoor[a]

[a]*Department of Chemistry, Arak Branch, Islamic Azad University, Arak, Iran, Tel. +989111321210,*
email: sanaz_toutounchi@yahoo.com (S. Toutounchi), Tel. +0989380899935, email: k-mahanpoor@iau-arak.ac.ir (K. Mahanpoor)
[b]*Department of Chemistry, Rasht Branch, Islamic Azad University, Rasht, Iran, Tel./Fax +981333402718,*
email: shariaty@iaurasht.ac.ir (S. Shariati)

ABSTRACT

In the present study, the synthesis of a new type of sulfonic acid functionalized magnetite ordered nanomesoporous carbon (Fe_3O_4@SiO_2-CMK-8/SO_3H NPs) was carried out by carbonizing sucrose inside the pores of the KIT-6 mesoporous silica. The synthesized nano particles were characterized by XRD, FT-IR and SEM instruments and then applied to investigate the removal of hazardous Safranin O dye from aqueous solutions. The size of synthesized nanomesoporous carbon was obtained as lower than 40 nm with spherical shape. Taguchi experimental design method (OA_{16}) was used to evaluate the effect of adsorption experimental parameters on the dye removal efficiency from aqueous solutions. At the optimum condition (adsorption amount = 0.06 g (2.4 g L^{-1}), pH = 6, ionic strength = 0.05 mol L^{-1} and contact time = 30 min), the adsorption of Safranin O from aqueous solutions was found to be better than 93.0%. Kinetic studies were performed at two concentrations (25 and 100 mg L^{-1}) using four known kinetic models including pseudo-first-order, pseudo-second-order, intra-particle-diffusion and Elovich models and data were obeyed well from pseudo-second-order kinetic model (R^2 = 0.999). Analysis of equilibrium adsorption data with Freundlich, Langmuir and Temkin isotherms revealed that the adsorption data were best fitted to Freundlich model (R^2 = 0.9941, n = 2.07) rather than Langmuir (R^2 = 0.9526, q_{max} = 88.50 mg g^{-1}) and Temkin (R^2 = 0.7894) isotherms. Analysis of real samples showed the successive removal of Safranin O dye from aqueous matrixes. In addition, the Fe_3O_4@SiO_2-CMK-8/SO_3H NPs could be simply recovered by external magnet and it exhibited recyclability and reusability for subsequent six runs.

Keywords: Magnetic nanoparticles; Safranin O; Sulfonic acid; Ordered nanomesoporous carbon; Adsorption

1. Introduction

There is rising public concern over the contamination of wastewater by dyes due to the fact that presence of dyes and pigments in water, even at very low concentrations, is very undesirable for both toxicological and aesthetic reasons [1–3]. Recently, extensive studies have been performed on mesoporous carbon materials as a good candidate for adsorption of dye pollutants from water [4–6]. Ordered mesoporous carbons of CMK-n (n = 1–9) with large surface area and high specific pore volume, along with tunable pore size have been of wide interest for applications in many areas such as adsorbents, catalyst supports, and materials for advanced electronic applications [7–12]. These materials were synthesized using well-ordered hexagonal and cubic mesoporous silica materials as hard frameworks and a carbon source [13,14].

In recent years, magnetic iron oxide nanoparticles (NPs) have received great potential applications in electronics, optoelectronics, medicine, magnetic storage and cleanup of environmental contaminants [15–19]. However, non-protected iron oxide NPs are sometimes unstable, and readily oxidize in air. Therefore, in order to immobilize and stabi-

*Corresponding author.

lize the iron oxide NPs, they could be embedded into a host matrix. In this way, by merging the CMK-n with magnetic iron oxide NPs, it is possible to extend new carbon hybrids with improved properties through synergetic effects. From the environmental attitude, such magnetic mesoporous hybrids could be utilized as adsorbents with a high efficiency because of their superior ability for adsorption and removal of various types of pollutants. In addition, these magnetic mesoporous adsorbents can be easily separated and collected by an external magnetic field [20–22].

In the present work, we prepared magnetite hybrids from silica coated iron oxide NPs and three-dimensional cubic ordered mesoporous carbon (CMK-8) using the high-quality large ordered mesoporous cubic Ia3d silica KIT-6 as the template, sucrose as the carbon source and Na_2SO_4 for insertion of the sulfonic acid groups. The final hybrid materials (Fe_3O_4@SiO_2-CMK-8/SO_3H NPs) were comparatively examined for their ability to remove Safranin O dye (SO) from aqueous solutions. SO is a cationic phenazine dye widely used in many foods for flavoring and coloring agents and in textile industries in dyeing cotton, wool, silk, leather and paper and also in staining and biological applications. Unfortunately, it is considered as a major pollutant, since it is toxic and carcinogenic to humans and animals [23]. Furthermore, SO dye is highly soluble in water and exerts toxic effects on biological systems. Hence, the removal of SO from the aqueous solutions is attractive. Here, the effect of experimental factors on SO dye removal efficiency including pH, contact time, the sorbent amount and ionic strength were studied using Taguchi fractional factorial design method. Also, the kinetic data, adsorption isotherms and removal of SO from different real samples were performed to demonstrate the efficiency of this adsorbent.

2. Experimental

2.1. Materials and reagents

The following reagents were purchased from Merck (Darmstadt, Germany) and used without further modification: ferric chloride hexahydrate ($FeCl_3 \cdot 6H_2O$), ferrous chloride tetrahydrate ($FeCl_2 \cdot 4H_2O$), ammonia (NH_3, 25 wt%), tetraethyl orthosilicate (TEOS), sucrose, and *n*-butanol. Pluronic P123 (EO_{20}-PO_{70}-EO_{20}, M_w = 5800) and Safranin O (SO, $C_{20}H_{19}N_4Cl$, 3,7-diamino-2,8-dimethyl-5-phenyl-phenazinium chloride, C.I. Basic Red 2, M_w = 350.84 g mol^{-1}) were purchased from Sigma-Aldrich (Milwaukee, WI, USA) and BDH chemicals (Poole, England).

2.2. Apparatus

The crystal structure of prepared Fe_3O_4@SiO_2-CMK-8 NPs was investigated by X-ray diffraction (XRD) using Phillips (pw-1840) X-ray diffractometer with Cu-Kα radiation source (λ = 1.54056 Å) at 40 KV voltage and 25 mA current in a wide - angle range (2θ = 5–80). FT-IR spectroscopy was carried out using a Shimadzu FT-IR spectrophotometer (model 470, Japan) by using KBr pellets. The surface morphology was studied using a Philips XL 30 scanning electron microscope (SEM, The Netherlands). A digital Bante pH meter (model 930, China) equipped with a combined

glass electrode was applied to adjust the pH of solutions. The UV-Vis absorption measurements were carried out by a MAPADA UV-Vis spectrophotometer (6300 pc series, China). For magnetic separation a strong magnet (1×3×5 cm) with 1.4 T magnetic field was applied. A magnetic stirrer (Labinco, The Netherlands) and a stirrer bar (4 × 14 mm) were used to enhance mass transfer of SO from the solution to the surface of adsorbent.

2.3. Standard curve of SO

The SO dye stock solution with 50 mg L^{-1} concentration was prepared by dissolving 50.0 mg of SO dye in distilled water in a 1 L volumetric flask. The working solutions were obtained by diluting the dye stock solution in accurate proportions to needed initial concentrations (0.1–25 mg L^{-1}). The calibration curve was characterized by a high correlation coefficient (R^2 = 0.9997) at pH = 6 using UV-Vis spectrophotometer (λ = 517 nm).

2.4. Preparation of magnetic Fe_3O_4@SiO_2@KIT-6 NPs

For synthesis of Fe_3O_4@SiO_2-KIT-6 NPs, firstly, the Fe_3O_4 NPs were prepared by co-precipitation reaction of chloride salts of the Fe^{3+} and Fe^{2+} ions with molar ratio 2:1 in the presence of ammonia solution. The black magnetite NPs were coated with silica layer via a sol-gel method [24–26]. Then, mesoporous magnetite NPs of Fe_3O_4@SiO_2@KIT-6 were synthesized according to reported following procedure [26]: typically, 1.25 g of Pluronic P123 copolymer was dissolved in 45 mL of distilled water under vigorous stirring at 35°C. After complete dissolution, 1.3 mL of HCl solution (35%) and 1.5 mL of *n*-butanol (99.4%) were mixed. Following additional stirring for 1 h, 1 g premade Fe_3O_4@SiO_2 was added to reaction vessel and mixed for 1 h. Subsequently, 2.7 mL of TEOS was added immediately. The mixture was left stirring at room temperature (r.t) for 24 h and transferred into an autoclave that was sealed and maintained at 110°C for another 24 h under static conditions. The resulting product was separated magnetically, washed with EtOH/H_2O several times (3 × 50 mL) and then dried at 80°C for 10 h [26,27]. The final sample was calcined at 550°C for 6 h in air to achieve an orange powder as the framework for synthesis of ordered mesoporous carbon materials.

2.5. Preparation of magnetic Fe_3O_4@SiO_2-CMK-8 NPs

In general, 0.04 g H_2SO_4 and 1.25 g sucrose were added to 5 mL deionized water. The mixture was mixed with 1 g Fe_3O_4@SiO_2@KIT-6 NPs. The mixture was dried in an oven at 100°C for 6 h. The temperature was increased to 160°C and preserved for another 6 h. Again, sucrose solution (prepared with 0.75 g sucrose and 0.08 g H_2SO_4 in 5 mL H_2O) was added to the partially polymerized and carbonized sucrose and the drying process was repeated. The sample turned to dark brown during the treatment in the oven. The carbonization was completed in flowing argon gas at 800°C for 5 h to achieve black powder of Fe_3O_4@SiO_2@KIT-6@CMK-8 [28]. To eliminate the silica template, the prepared composite (Fe_3O_4@SiO_2@KIT-6@CMK-8) was washed by ethanolic NaOH 1 M (EtOH-H_2O, 50:50 v/v), filtered and washed

with distilled water. Finally, the Fe_3O_4@SiO_2-CMK-8 NPs were dried at 100°C for 12h.

2.6. Preparation of magnetic Fe_3O_4@SiO_2-CMK-8/SO_3H NPs

The obtained Fe_3O_4@SiO_2-CMK-8 NPs (0.15 g) were ultrasonically dispersed in 10 mL of distilled water containing 0.35 g of Na_2SO_4 (10 min). Then, the mixture was stirred for 2 h at r.t for insertion of sulfonic acid groups. The resulting product was collected by a magnet and washed with distilled water and then dried in the oven at 80°C for 10 h.

2.7. Taguchi method

For optimization of the SO removal by the Fe_3O_4@SiO_2-CMK-8/SO_3H NPs, Taguchi fractional factorial design method (OA_{16}) was used to determine the optimal conditions [29]. This study considers four levels for four controllable factors including solution pH, adsorption amount, contact time and ionic strength. Therefore, Taguchi OA_{16} (4^4) was chosen (Table 1) that required 16 experiments to complete the optimization process and the average of absorbance responses for each factor at different levels were calculated. For optimizing the experimental parameters, all experiments were done with 25 mg L^{-1} concentration of SO samples (25 mL).

2.8. Adsorption studies

The primary UV-Vis spectrophotometric measurements were carried out in different pHs to find the stability of SO spectral absorbance. The results showed that SO dye was stable in all the studied ranges of pHs. For adsorption process, batch experiments were carried out to evaluate the adsorptive removal of SO. Experiments were conducted using 25 mL solutions containing 25 mg L^{-1} SO to elucidate the varying several conditions such as solution pH (6–9), adsorbent amount (0.06–0.12 g), contact time (5–30 min) and ionic strength (0–0.05 mol L^{-1}). The pH of the solutions was adjusted by dropwise addition of 0.1 M HCl or 0.1 M NaOH solutions. After each removal experiments, the NPs were separated from the dye solutions with a permanent magnet and the residual concentrations of SO in the solutions were determined by UV-Vis spectrophotometer at 517 nm.

3. Results and discussion

In continuation to our prior works [29–33], herein, the modified magnetic Fe_3O_4@SiO_2-CMK-8/SO_3H NPs were synthesized by the following steps (Fig. 1). Firstly, Fe_3O_4 NPs

Table 1
The OA_{16} matrix for optimization the experimental parameters

EX. no	Exp. order	Time (min)	Ionic strength (mol L^{-1})	Adsorption amount (g)	pH
1	10	15	0.05	0.08	8
2	7	5	0.05	0.1	7
3	14	5	0.01	0.08	9
4	5	15	0.005	0.06	7
5	3	15	0.01	0.1	6
6	13	10	0.05	0.06	9
7	12	5	0.005	0.12	8
8	2	10	0.005	0.08	6
9	6	30	0	0.08	7
10	4	30	0.05	0.12	6
11	9	30	0.01	0.06	8
12	1	5	0	0.06	6
13	11	10	0	0.1	8
14	15	30	0.005	0.1	9
15	16	15	0	0.12	9
16	8	10	0.01	0.12	7
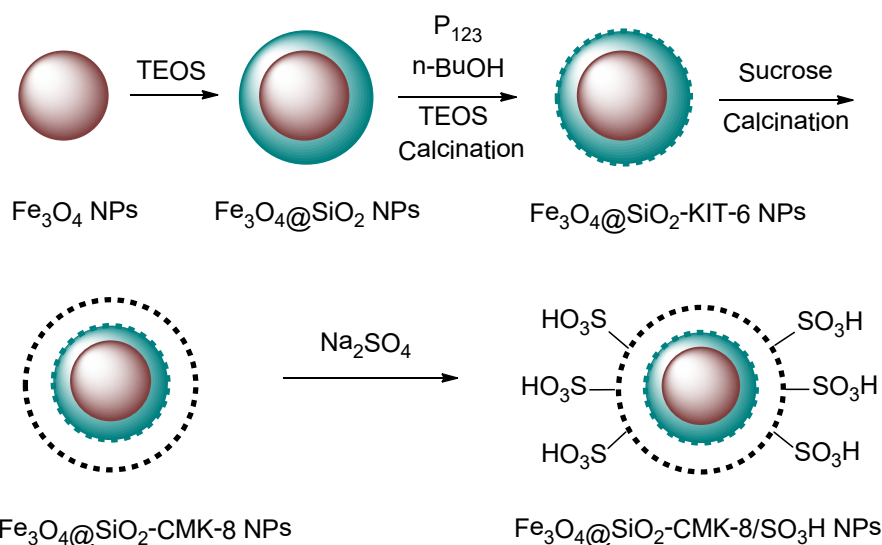
Fig. 1. Preparation of Fe_3O_4@SiO_2-CMK-8/SO_3H NPs.

were prepared by co-precipitation of Fe^{2+} and Fe^{3+} ions in basic solution and then in order to avoid possible aggregation or oxidation of the Fe_3O_4 NPs, a layer of SiO_2 was coated on the surface of Fe_3O_4 NPs using sol-gel process, through the hydrolysis of TEOS. Then, $Fe_3O_4@SiO_2$ core-shell nanoparticles were successfully prepared. Subsequently, $Fe_3O_4@SiO_2$ core-shell NPs were coated with KIT-6 to obtain highly ordered large pore $Fe_3O_4@SiO_2@KIT$-6 NPs. Mesoporous silica KIT-6 template was firstly prepared according to the published procedure using a mixture of pluronic P123 and *n*-butanol [30]. After that, KIT-6 and sucrose were used as the template and the carbon precursor, respectively to obtain $Fe_3O_4@SiO_2$-CMK-8NPs. Finally, $Fe_3O_4@SiO_2$-CMK-8/SO_3H NPs were prepared by the reaction of $Fe_3O_4@SiO_2$-CMK-8 NPs with Na_2SO_4 for formation of sulfonic acid groups onto $Fe_3O_4@SiO_2$-CMK-8 surface and the success of this immobilization was confirmed with FT-IR spectra.

3.1. Structural characterization

The FT-IR spectra of (a) Fe_3O_4 NPs, (b) $Fe_3O_4@SiO_2$ NPs, (c) $Fe_3O_4@SiO_2@KIT$-6 NPs, (d) $Fe_3O_4@SiO_2$-CMK-8 NPs and (e) $Fe_3O_4@SiO_2$-CMK-8/SO_3H NPs were shown in (Fig. 2). The absorption band for Fe_3O_4 NPs at 572 cm^{-1} is attributed to the stretching vibration of Fe-O bond and two bands at 3454 and 1631 cm^{-1} are related to the symmetric and asymmetric stretching and bending vibrations of O-H, respectively which is attached to the surface iron atoms. For $Fe_3O_4@SiO_2$ NPs (Fig. 2b) and $Fe_3O_4@SiO_2@KIT$-6 NPs (Fig. 2c), the strong broad bands in 1089 and 1087 cm^{-1} with a shoulder at 1209 cm^{-1} are assigned to the asymmetric stretching vibrations of Si-O-Si in SiO_2. The weaker bands at 796, 466 and 952 cm^{-1} are corresponded to the Si-O-Si symmetric stretching vibrations, Si-O-Si or O-Si-O bending modes and Si-O symmetric stretching vibrations, respectively. In both spectra of $Fe_3O_4@SiO_2$-CMK-8 NPs (Fig. 2d) and $Fe_3O_4@SiO_2$-CMK-8/SO_3H NPs (Fig. 2e), the similar signals for
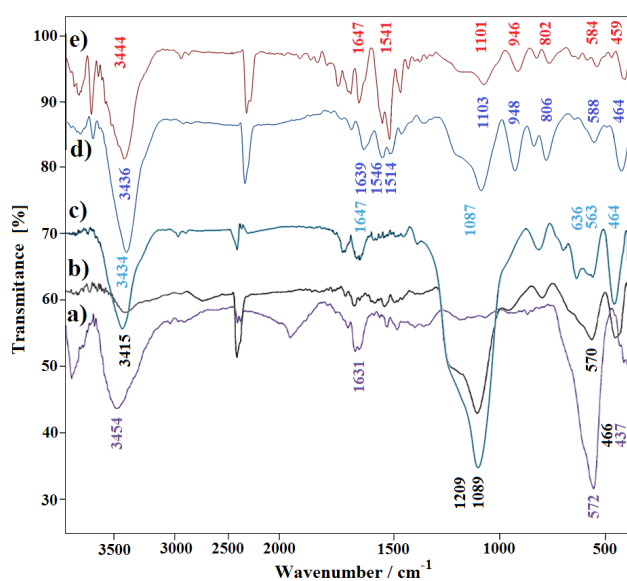
Fe_3O_4 at 464 and 459 cm^{-1} are related to the stretching vibrations of Fe-O bond and two bands in both spectra at 3436, 1639 cm^{-1} and 3444, 1647 cm^{-1} are related to the symmetric and asymmetric stretching and bending vibrations of O-H, respectively. The broad bands in both spectra in 1101 and 1103 cm^{-1} with a shoulder are allocated to the asymmetric stretching vibrations of Si-O-Si. In the $Fe_3O_4@SiO_2$-CMK-8/SO_3H NPs (Fig. 2e), this absorption band is broadened and overlapped with the bands at 1161.2 and 1032 cm^{-1} that are attributed to SO_3^- stretching and O=S=O stretching vibrations in SO_3H group.

The morphology and size of the $Fe_3O_4@SiO_2$-CMK-8/SO_3H NPs were investigated by SEM instrument as shown in Fig. 3. The SEM images demonstrate that the particles have spherical shape and seem to be nanosized (<40 nm). In addition, the XRD pattern of $Fe_3O_4@SiO_2$-CMK-8 NPs (Fig. 4c) was compared with Fe_3O_4 NPs (Fig. 4a) and $Fe_3O_4@SiO_2$ NPs (Fig. 4b) that were shown in Fig. 4. The sharp diffraction peaks with 2θ at 30.4°, 35.6°, 43.4°, 53.8°, 57.3°, 62.6° and 71° which are quite identical to pure magnetite and matched well with the XRD pattern of the standard Fe_3O_4 from Joint Committee on Powder Diffraction Standards (JCPDS No.19–692), confirmed the presence of magnetite core in the structure of synthesized mesoporous carbon (Fig. 4 a). XRD

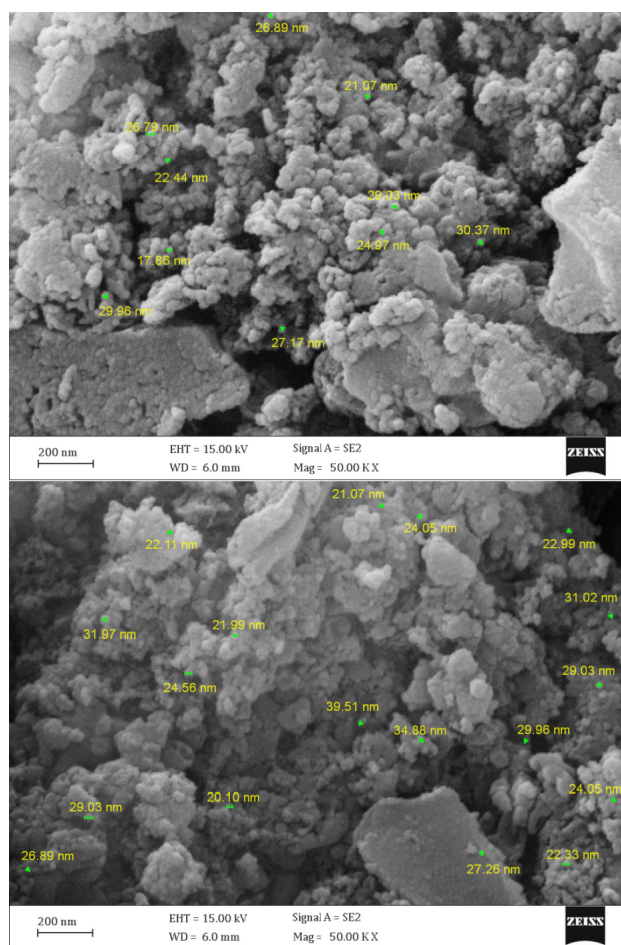Fig. 2. The FT-IR spectra of (a) Fe_3O_4 NPs, (b) $Fe_3O_4@SiO_2$ NPs, (c) $Fe_3O_4@SiO_2@KIT$-6 NPs, (d) $Fe_3O_4@SiO_2$-CMK-8 NPs and (e) $Fe_3O_4@SiO_2$-CMK-8/SO_3H NPs.

Fig. 3. The SEM images of synthesized $Fe_3O_4@SiO_2$-CMK-8/SO_3H NPs.
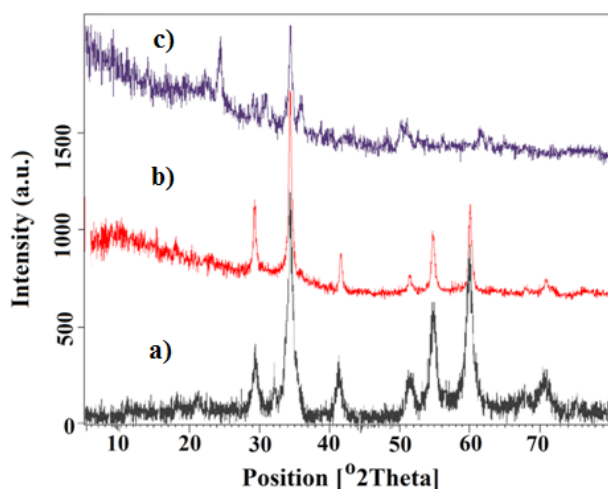
Fig. 4. The XRD patterns of (a) Fe_3O_4 NPs, (b) Fe_3O_4@SiO$_2$ NPs and (c) Fe_3O_4@SiO$_2$-CMK-8 NPs.

Fig. 5. Variation of SO removal efficiency with solution pHs($[SO]_0$ = 25 mg L^{-1}).

pattern indicates that the Fe_3O_4 core has crystalline cubic spinel structure. Figs. 4 a–c shows the crystalline phase of Fe_3O_4 NPs was stable during silica coating and surface carbonization. Decrease in intensities of diffraction peaks of Fe_3O_4 in Figs. 4b,c results from SiO$_2$ coating (Fig. 4b). The decrease is serious after formation of carbon mesoporous structure (Fig. 4c) due to the absorption of X-ray through the shells.

3.2. Effect of solution pH on the SO removal efficiency

The pH of the aqueous solution is an important parameter that affects the adsorption properties of adsorbent and adsorbate via changing the surface charge of adsorbent and the degree of ionization and speciation of SO molecules. Prior to optimization steps, the effect of solution pH on the SO removal efficiency was studied by changing the pH of solution from 3 to 11. According to the results, at pHs lower than 6 and higher than 9, the removal efficiency was decreased (Fig. 5). Therefore, in optimization steps, pH levels were investigated in the range of 6–9. The adsorption process can be explained by electrostatic interactions between cationic SO dye and anionic SO_3^- groups on the surface of Fe_3O_4@SiO$_2$-CMK-8/SO$_3$H NPs [34]. The decrease in removal efficiency in higher pHs, can be related to the reduction in positive charge of SO dye. According to the optimization results, as the solution pH increased from 6 to 9, SO removal dropped from 92.0% to 88.0% which could be attributed to the decreasing of electrostatic attractions between the SO and Fe_3O_4@SiO$_2$-CMK-8/SO$_3$H NPs. Accordingly, the highest dye adsorption was obtained at pH = 6. Therefore, this pH was selected as the optimum value for other experiments. This result is in agreement with our previous study on the adsorption of SO by sulfonic acid functionalized SBA-3 silica mesoporous magnetite nanocomposite (Fe_3O_4@SiO$_2$@SBA-3/SO$_3$H) [35].

3.3. Effect of adsorbent amount on the SO removal efficiency

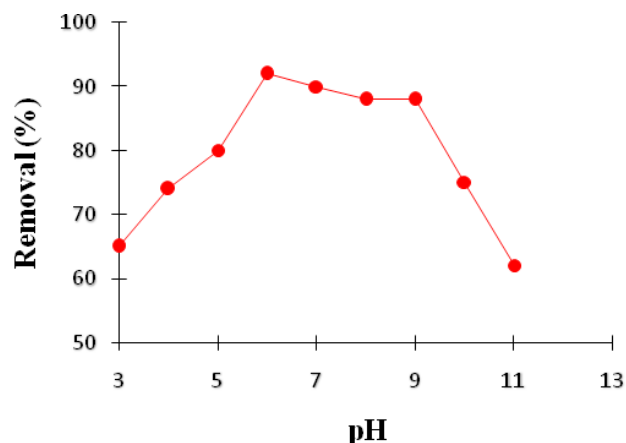Adsorbent amount is a key factor in the adsorption treatment that determines the capacity of an adsorbent for dye removal. Here, the adsorption of SO dye on the surface of Fe_3O_4@SiO$_2$-CMK-8/SO$_3$H NPs was investigated by changing the quantity of adsorbent in the range of 0.06, 0.08, 0.10 and 0.12 g (2.4 g L^{-1} to 4.8 g L^{-1}) with the dye concentration of 25 mg L^{-1}at r.t (25°C). The results (Fig. 6), show that with increase in the adsorbent amount from 0.06 to 0.12 g, the SO removal efficiency decreases. High adsorbent dosage can be caused to excess particle interactions, such as aggregation that would lead to decrease in the total surface area of the adsorbent [36].

3.4. Effect of ionic strength on the SO removal efficiency

To investigate the effect of salts that presents in solution, the effect of ionic strength was carried out using different concentrations of NaCl (0, 0.005, 0.01 and 0.05 mol L^{-1}). The data obtained confirmed that; the SO removal efficiency was better at 0.05 mol L^{-1} NaCl (Fig. 7). This effect may be due to the decrease in solubility of the SO dye in water and enhancement of the hydrophobic interaction between SO and the surface of Fe_3O_4@SiO$_2$-CMK-8/SO$_3$H NPs in the presence of salt that result an increase in dye removal efficiency [37]. Thus, all further experiments were considered in the NaCl concentration of 0.05 mol L^{-1}.

3.5. Effect of contact time on the SO removal efficiency

To know the equilibration time for obtaining maximum SO removal, the adsorption of SO on the surface of Fe_3O_4@SiO$_2$-CMK-8/SO$_3$H NPs was studied at different contact times in the range of 5–30 min and the absorbance of the residual dye solution was recorded at λ_{max} (517 nm, Fig. 8). It was observed that the adsorption of dye increased in contact time of 30 min, and attained a constant value at equilibrium after a specific time. Also, after optimization by Taguchi method, the contact time of 45 min was compared by 30 min, and it was found that the removal efficiency was relatively constant respect to 30 min (Fig. 8). Therefore, 30 min was preferred as the optimum contact time for all further adsorption experiments.

To study the SO removal efficiency at obtained optimum conditions (adsorbent amount = 0.06 g, pH = 6, contact time
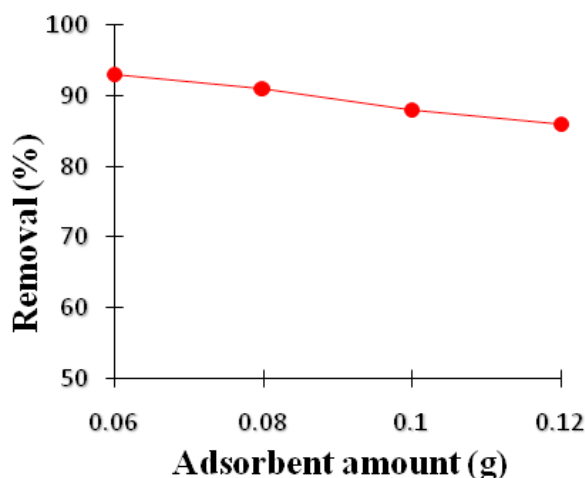
Fig. 6. The effect of adsorbent amount on the adsorption of SO on $Fe_3O_4@SiO_2$-CMK-8/SO_3H NPs ($[SO]_0$ = 25 mg L^{-1}).
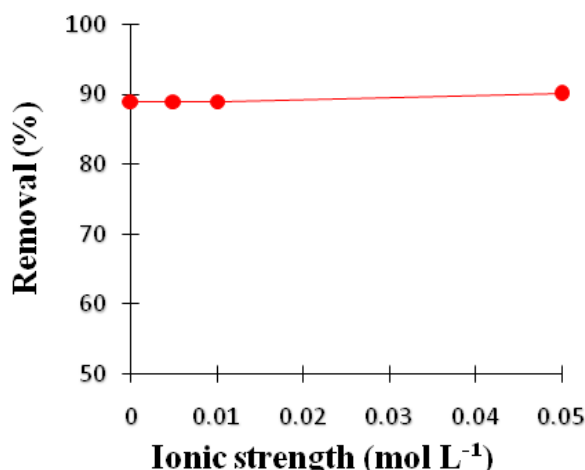
Fig. 7. Effect of ionic strength on the adsorption of SO on the $Fe_3O_4@SiO_2$-CMK-8/SO_3H NPs.
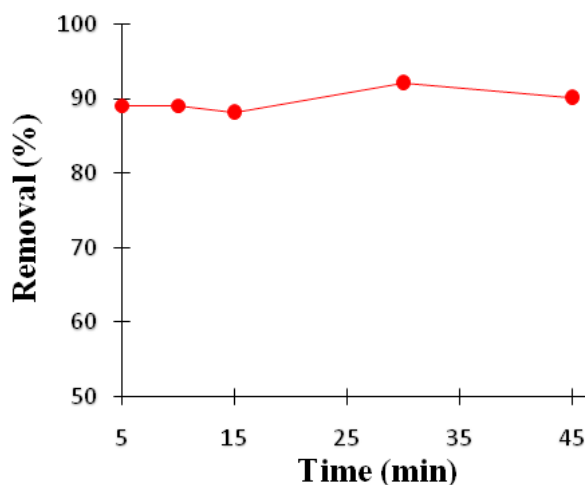
Fig. 8. The effect of contact time on the adsorption of SO on the $Fe_3O_4@SiO_2$-CMK-8/SO_3H NPs.

= 30 min and ionic strength = 0.05 mol L^{-1}), six replicative experiments were carried out at optimum conditions and the SO removal efficiencies were found to be better than 93.0% with a relative standard deviation of 0.94% (RSD %) that show the very good repeatability of the results.

3.6. Study of adsorption kinetics

The adsorption kinetic describes helpful data about efficiency of adsorption, solute adsorption rate and pathway. Adsorption kinetic experiments were performed at two different SO concentrations of 25 and 100 mg L^{-1}, at obtained optimum conditions (adsorbent amount = 0.06 g, pH = 6 and ionic strength = 0.05 mol L^{-1}) in the range of 0–90 min. The pseudo first-order, pseudo second-order, intra-particle diffusion and Elovich models were investigated in order to find an efficient kinetic model for the description of adsorption kinetic. The pseudo first-order kinetic model is expressed as follow [38]:

$$\ln\left(q_e - q_t\right) = \ln\left(q_e\right) - k_1 t \tag{1}$$

where q_e and q_t (mg g^{-1}) are the adsorption capacities at equilibrium and at time t (mg g^{-1}), respectively; k_1 (min^{-1}) is the rate constant of the pseudo first-order adsorption. The values of k_1 and q_e were obtained from the slope and intercept of the plot of ln $(q_e - q_t)$ versus t, respectively.

The pseudo second-order kinetic model was presented below [39]:

$$\frac{t}{q_t} = \frac{1}{k_2 q_e^2} + \left(\frac{1}{q_e}\right)t \tag{2}$$

where k_2 is the pseudo second-order adsorption constant (g mg^{-1} min^{-1}). The intercept of the plot of $\frac{t}{q_t}$ against t gives the second-order rate constant k_2.

The possibility of intra-particle diffusion resistance affecting adsorption was examined by the intra-particle diffusion model as [40]:

$$q_t = k_p t^{1/2} + C \tag{3}$$

where k_p (mg g^{-1} min$^{-1/2}$) is the intra-particle diffusion rate constant which can be calculated from the slope of the linear plot of q_t against $t^{1/2}$, and C (mg g^{-1}) is intercept. Value of C presents a plan about the thickness of the boundary layer: the larger the intercept, the greater the boundary layer effect.

The Elovich equation is given below:

$$\frac{dq_t}{dt} = \alpha e^{-\beta q_t} \tag{4}$$

The integration of the rate equation with the same boundary conditions as the pseudo first-and second-order equations becomes the Elovich equation [41].

$$q_t = \frac{1}{\beta}\ln\left(\alpha\beta\right) + \frac{1}{\beta}\ln\left(t\right) \tag{5}$$

where α is the initial adsorption rate (mg g^{-1} min^{-1}), and β is related to the extent of surface coverage (g mg^{-1}).

Table 2
Kinetic parameters for SO adsorption onto $Fe_3O_4@SiO_2$-CMK-8/SO_3H NPs

Kinetic models	$[SO]_0$	
	25	100
Pseudo first-order		
k_1 (min^{-1})	0.0395	0.0067
$q_{e,cal}$ (mg g^{-1})	9.80	31.79
R^2	0.124	0.736
Pseudo second-order		
k_2 (g mg^{-1} min^{-1})	0.2719	0.0108
$q_{e,cal}$ (mg g^{-1})	10.1214	4.4937
R^2	0.9998	0.9985
Intra-particle diffusion		
K_P (mg g^{-1} min$^{-1/2}$)	0.5149	2.1601
C_0 (mg g^{-1})	6.7137	23.5001
R^2	0.3839	0.8898
Elovich		
α (mg g^{-1} min^{-1})	139.5300	463.0200
b (g mg^{-1})	0.8116	0.2173
R^2	0.5345	0.9809

The best-fit model was selected based on the linear regression correlation coefficient (R^2 values). The kinetic parameters for the SO removal at two different concentrations by four models are summarized in Table 2. The results show that intra-particle diffusion and Elovich models are not suitable for the present adsorption system due to low correlation coefficients (R^2). The kinetic data for SO adsorption showed the best fitting ($R^2 > 0.99$) with the pseudo second-order model. Moreover, when the initial SO concentration increased from 25 to 100 mg L^{-1}, the value of k_2 (g mg^{-1} min^{-1}) and (R^2) for the pseudo second-order model were decreased from 0.2719 to 0.0108 g mg^{-1} min^{-1} and 0.9998 to 0.9985, respectively. Also, $q_{e,cal}$ (mg g^{-1}) reduced from 10.1214 to 4.4937 mg g^{-1}. This result indicated that adsorption data were in agreement with this model. Furthermore, the curve-fitting plots of pseudo second-order kinetic model gave a straight line, passed through the origin and confirmed the best fit of this kinetic model in the present system (Fig. 9). For the intra-particle diffusion model the value of C was estimated as 6.7137 mg g^{-1} ($C \neq 0$) that confirms intra-particle diffusion is not the only rate-limiting step for SO adsorption.

3.7. Studies of adsorption isotherms

In order to evaluate the adsorption isotherms of the SO adsorption on the surface of NPs, different SO concentrations were fitted to three most widely used equilibrium adsorption isotherm models namely Freundlich, Langmuir [42] and Temkin. Both Freundlich and Langmuir models are suitable for adsorption on heterogeneous surfaces. For isotherm studies, SO solutions with 1 to 500 mg L^{-1} concentrations were used. The study of adsorption
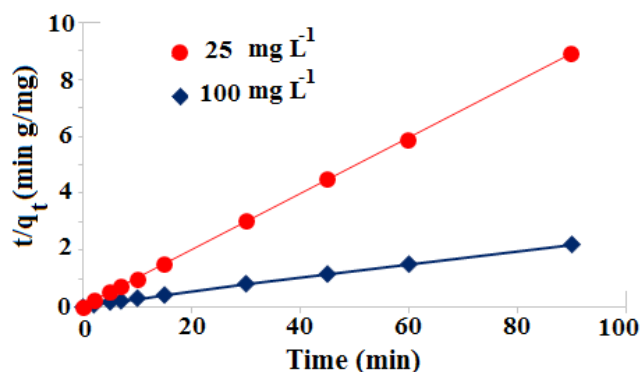

Fig. 9. The linear plots of pseudo second-order model on the SO removal by $Fe_3O_4@SiO_2$-CMK-8/SO_3H NPs in different time and concentrations (pH = 6, adsorbent amount = 0.06 g and ionic strength = 0.05 mol L^{-1}).

isotherms of SO on the $Fe_3O_4@SiO_2$-CMK-8/SO_3H NPs at optimum conditions (adsorbent amount= 0.06 g at pH = 6, r.t) are given in Fig. 10. The Langmuir isotherm supposes that monolayer adsorption occurs at binding sites with homogenous energy levels, without interactions between adsorbed molecules and transmigration of adsorbed molecules onto the adsorption surface. The Langmuir equations can be expressed as [43]:

$$q_e = \frac{q_m k_l C_e}{1 + k_l C_e} \tag{6}$$

or

$$\frac{C_e}{q_e} = \frac{1}{k_l q_m} + \frac{1}{q_m} C_e \tag{7}$$

where C_e is the function of equilibrium concentration of the SO solution (mg L^{-1}), q_e is the adsorption capacity (mg g^{-1}), k_l is the constant correlated to free energy of adsorption (L mg^{-1}), and q_m is the maximum adsorption capacity (mg g^{-1}).

The Freundlich isotherm is commonly represented by [44]:

$$q_e = k_f C_e^{1/n} \tag{8}$$

or

$$\ln q_e = \ln k_f + \frac{1}{n} \ln C_e \tag{9}$$

where K_f (mg$^{1-(1/n)}$ L$^{1/n}$ g^{-1}) is Freundlich adsorption constant, n is constant parameter of the system. If the value of $1/n$ is lower than 1, it illustrates a normal Freundlich isotherm; if not, it is indicative of supportive adsorption [45].

Temkin isotherm contains a factor that obviously is taking into the account of adsorbent-adsorbate interactions. By ignoring the extremely low and large concentrations, the model assumes that heat of adsorption of all molecules in the layer would decrease linearly than logarithmic binding energies [46,47]. This isotherm is usually used for heterogeneous surface systems or non-uniform distribution of sorption heat. The model is given by the following equations [46]:
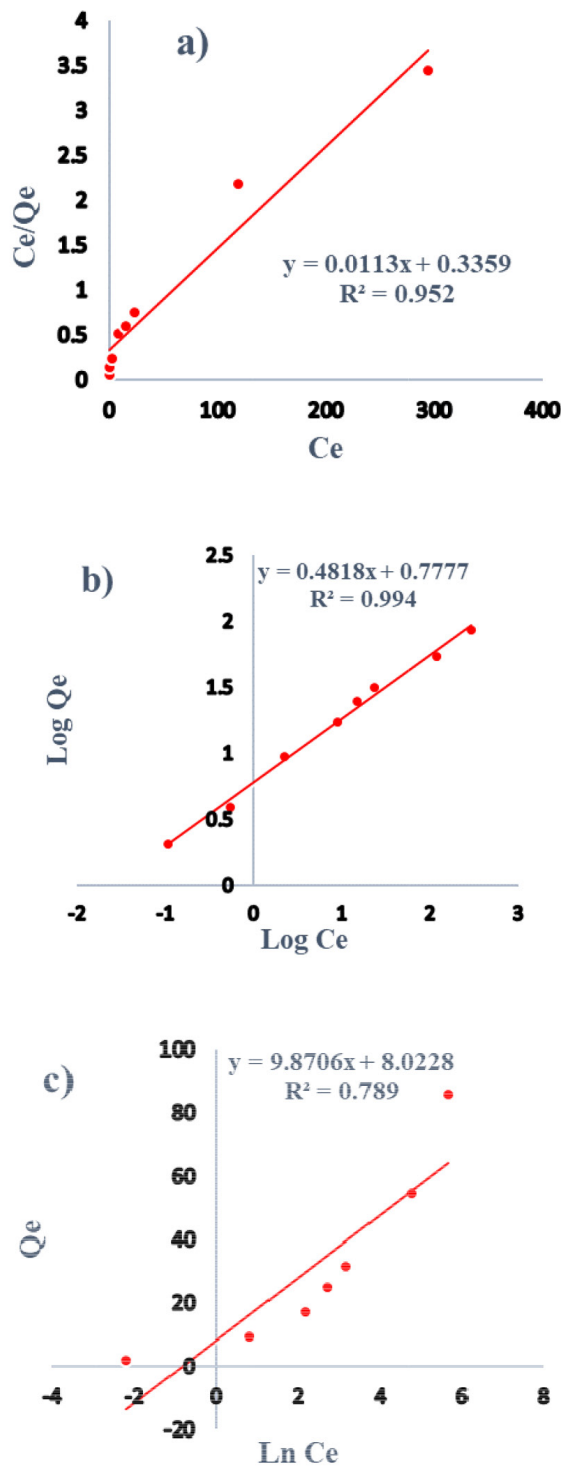
Fig. 10. The plots of (a) Langmuir (b) Freundlich and (c) Temkin isotherms on the SO removal by $Fe_3O_4@SiO_2$-CMK-8/SO_3H NPs (pH = 6, [SO]$_0$ = 25 mg L^{-1}, adsorbent amount = 0.06 g and ionic strength = 0.05 mol L^{-1}).

$$ln(AC_e) = \frac{RT}{b}q_e \tag{10}$$

Table 3
Adsorption isotherm parameters for SO adsorption on the $Fe_3O_4@SiO_2$-CMK-8/SO_3H NPs

Isotherm models	
Langmuir	
q_m (mg g^{-1})	88.4955
k_1 (L mg^{-1})	0.0336
R^2	0.9526
Freundlich	
K_f (mg$^{1-(1/n)}$ L$^{1/n}$ g^{-1})	5.9937
N	2.07
R^2	0.9941
Temkin	
b (J mol^{-1})	9.8706
A (L g^{-1})	2.255
R^2	0.7894

$$\ln C_e + \left(\frac{RT}{b}\right)\ln A \frac{RT}{b} = q_e \tag{11}$$

$$B = \frac{RT}{b}$$

$$q_e = B \ln A + B \ln C_e \tag{12}$$

where, A is Temkin isotherm equilibrium building constant (L g^{-1}), b is constant related to heat of sorption (J mol^{-1}) and B is Temkin isotherm constant.

The calculated isotherm parameters by means of a non-linear fitting procedure are shown in Table 3. The adsorption of SO was best fitted with the Freundlich isotherm model with the higher R^2 (0.994). Therefore, SO adsorption onto $Fe_3O_4@SiO_2$-CMK-8/SO_3H NPs surface was multilayer adsorption. The Freundlich constant $1/n$ was smaller than 1, representing a high adsorption intensity. In addition, the maximum monolayer adsorption capacity (q_m) of SO by $Fe_3O_4@SiO_2$-CMK-8/SO_3H NPs was obtained as 88.4955 mg g^{-1} in 298 K (Table 3).

3.8. Desorption and recycling studies

While SO adsorption on the surface of $Fe_3O_4@SiO_2$-CMK-8/SO_3H NPs is a reversible process, it is possible for regeneration or activation of adsorbent to reuse. The desorption of SO was carried out using HCl 0.1 M. The results showed that removal efficiency higher than 93% after six cycles can be attained in a short time of 1 min and in one elution step using 3 mL of HCl 0.1 M, as shown in Fig. 11. In fact, the SO molecules on the surface of $Fe_3O_4@SiO_2$-CMK-8/SO_3H NPs could be replaced with proton of the acidic solution in desorption step.

Furthermore, after seven cycles of the desorption-adsorption process, the high magnetic sensitivity of $Fe_3O_4@SiO_2$-CMK-8/SO_3H NPs still retained and the NPs can be collected from the solution using a super magnet (1.4 T, right inset in Fig. 11b). Therefore, the $Fe_3O_4@SiO_2$-

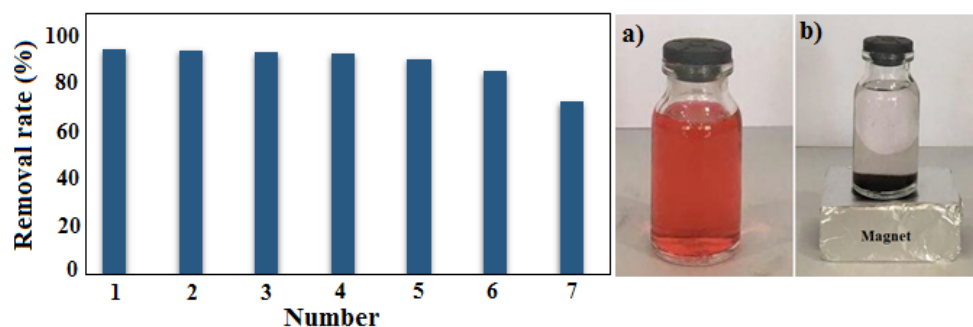Fig. 11. The removal efficiency during seven cycles of Fe_3O_4@SiO_2-CMK-8/SO_3H NPs. The inset figures show aqueous solutions of SO (a) before adsorption and (b) after seven cycles of desorption-adsorption.

CMK-8/SO_3H NPs can be potentially used as a recyclable magnetic adsorbent for further dye adsorption from water samples. The decrease in SO removal efficiency under removal cycles more than seven cycles, may be due to losing or deactivation of the adsorbent through the following steps.

3.10. Adsorption of SO in real samples

We studied the applicability and reliability of the Fe_3O_4@SiO_2-CMK-8/SO_3H NPs on four main sources that were collected from Caspian Sea, GhaleRoodkhan River, Pasikhan River and an industrial dyeing wastewater from Guilan, Iran. The chemical composition of four real samples including electrical conductivity (EC) at 20°C, pH, nitrate, nitrite, sulfate and chloride concentrations, total hardness (TH) and carbonate hardness (CH) were initially measured (Table 4). Prior to adsorption process, each real sample was analyzed to measure its dye content. Then, to determine the matrix effect on the SO removal efficiency, a known concentration of SO dye (25 mg L^{-1}) was added in real water samples and SO removal efficiency of proposed NPs was determined under optimized conditions (pH = 6, adsorbent amount = 0.06 g, contact time 30 min and ionic strength = 0.05 mol L^{-1}) by UV-Vis spectrophotometer. For each real sample, four adsorption experiments were carried out at optimum conditions and the results (Table 4) showed that SO removal efficiency in all of the samples, were better than 95% with good repeatability (RSD% lower than 1.4%). The results reveal the effectiveness of this method for removal of SO dye from real aqueous samples.

Table 5
Comparison of various adsorbents for SO removal

Adsorbents	q_m (mg g^{-1})	Ref.
SH[a]	29.49	[48]
MCM-41	68.80	[49]
ACCC[b]	1428.57	[50]
SBA-16	240.39	[51]
MR[M]Wc	89.40	[52]
NARM[W]d	9.77	[23]
NRKC[e]	16.23	[53]
CFA[f]	1.76	[54]
AC[g]	3.183	[55]
ARH[h]	0.2117	[55]
MWCNT/PU[i]	270.27	[56]
Fe_3O_4@CMK-8/SO_3H NPs	88.50	This work

[a]Soybean hull
[b]Activated carbon corncobs
[c]Modified red mud waste
[d]Neutralized activated red mud waste
[e]Natural raw kaolinite clay
[f]Coal fly ash
[g] Activated carbon
[h]Activated rice husks
[i] Multiwalled carbon nanotube-polyurethane

3.11. Comparison with other adsorbents

Table 5 shows a comparison between the proposed-Fe_3O_4@SiO_2-CMK-8/SO_3H NPs with various adsorbents

Table 4
Chemical composition of real samples and SO removal efficiency in real samples using Fe_3O_4@SiO_2-CMK-8/SO_3H NPs under optimum conditions (pH = 6, adsorbent dosage = 0.06 g, contact time 30 min and ionic strength = 0.05 mol L^{-1})

Sample	pH	EC	Cl^- (mg L^{-1})	NO_3^- (mg L^{-1})	NO_2^- (mg L^{-1})	SO_4^{2-} (mg L^{-1})	TH (mg L^{-1})	CH(mg L^{-1} $CaCO_3$)	Removal Efficiency (%)
Caspian Sea water	8.5	7.14 ms	5147	1.17	ND	837.86	3700	150	98.40
Industrial dyeing wastewaters	9.5	365 µs	213	3.27	<0.03	46.73	390	240	99.95
GhaleRoodkhan River	8.5	7.30 ms	4082	0.48	ND	874.77	3700	100	95.90
Pasikhan River	8.0	141.1 µs	159.75	0.855	ND	23.39	140	70	99.90

used for removal of SO dye [23,48–56]. According to the table, the Fe_3O_4@SiO_2-CMK-8/SO_3H NPs showed satisfactory removal performance as compared to other reported adsorbents. Therefore, it could be considered as a preferable and efficient adsorbent for removing dye contaminants. Furthermore, the magnetic properties of Fe_3O_4@SiO_2-CMK-8/SO_3H NPs make it more efficient adsorbent for the removal of SO from aqueous solutions.

4. Conclusion

Fe_3O_4@SiO_2-CMK-8/SO_3H NPs has been successfully prepared from mesoporous silica KIT-6 as the template, sucrose as the carbon source and Na_2SO_4 for insertion of the sulfonic acid function onto its surface and then used as a mesoporous carbon adsorbent for removal of SO dye from aqueous solutions. The magnetic properties of Fe_3O_4@SiO_2-CMK-8/SO_3H NPs make it a more potential adsorbent for the removal of dye from aqueous solutions. In addition, the adsorbent can be easily regenerated by HCl 0.1 M during 1 min and reused for subsequent runs up to six replicates without any reduction in adsorbent efficiency. Magnetic separation, good removal efficiency, short adsorption and desorption times and reusability are the most important advantages of the proposed adsorbent. The results from investigation on experimental and real samples showed that Fe_3O_4@SiO_2-CMK-8/SO_3H NPs could be considered as a potential adsorbent for removal of dye from water samples.

References

[1] P.K. Sukul, S. Malik, Removal of toxic dyes from aqueous medium using adenine based bicomponent hydrogel, RSC Adv., 3 (2013) 1902–1915.

[2] M. Ghaedi, E. Nazari, R. Sahraie, M.K. Purkait, Kinetic and isotherm study of Bromothymol Blue and Methylene blue removal using Au-NP loaded on activated carbon, Desal. Water Treat., 52 (2014) 5504–5512.

[3] A. Pourjavadi, M. Nazari, B. Kabiri, S.H. Hosseini, C. Bennett, Preparation of porous graphene oxide/hydrogel nanocomposites and their ability for efficient adsorption of methylene blue, RSC Adv., 6 (2016) 10430–10437.

[4] M. Baikousi, A.B. Bourlinos, A. Douvalis, T. Bakas, D.F. Anagnostopoulos, J. Tucek, K. Safarova, R. Zboril, M.A. Karakassides, Synthesis and characterization of γ-Fe_2O_3/carbon hybrids and their application in removal of hexavalent chromium ions from aqueous solutions, Langmuir, 28 (2012) 3918–3930.

[5] L. Chen, T. Ji, L. Mu, Y. Shi, L. Brisbin, Z. Guo, M.A. Khan, D.P. Young, J. Zhu, Facile synthesis of mesoporous carbon nanocomposites from natural biomass for efficient dye adsorption and selective heavy metal removal, RSC Adv., 6 (2016) 2259–2269.

[6] N. Mohammadi, H. Khani, V.K. Gupta, S. Agarwal, Adsorption process of methyl orange dye onto mesoporous carbon material-kinetic and thermodynamic studies, J. Colloid Interface Sci., 362 (2013) 457–462.

[7] L. Li, Z.H. Zhu, G.Q. Lu, Z.F. Yan, S.Z. Qiao, Catalytic ammonia decomposition over CMK-3 supported Ru catalysts: Effects of surface treatments of supports, Carbon, 45 (2007) 11–20.

[8] Q. Sui, J. Huang, Y. Liu, X. Chang, G. Ji, S. Deng, T. Xie, G. Yu, Rapid removal of bisphenol A on highly ordered mesoporous carbon, J. Environ. Sci., 23 (2011) 177–182.

[9] Z. Wu, P.A. Webley, D. Zhao, Comprehensive study of pore evolution, mesostructural stability, and simultaneous surface functionalization of ordered mesoporous carbon (fdu-15) by wet oxidation as a promising adsorbent, Langmuir, 26 (2010) 10277–10286.

[10] C. Govindasamy, W.J. Son, W.S. Ahn, Synthesis of mesoporous materials SBA-15 and CMK-3 from fly ash and their application for CO_2 adsorption, J. Porous. Mater., 16 (2009) 545–551.

[11] F. Lufrano, P. Staiti, Influence of the surface-chemistry of modified mesoporous carbon on the electrochemical behavior of solid-state supercapacitors, Energy Fuels., 24 (2010) 3313–3320.

[12] J. Zhang, L.B. Kong, J.J. Cai, Y.C. Luo, L. Kang, Nano-composite of polypyrrole/modified mesoporous carbon for electrochemical capacitor application, Electrochim. Acta., 55 (2010) 8067–8073.

[13] H.J. Shin, R. Ryoo, M. Kruk, M. Jaroniec, Modification of SBA-15 pore connectivity by high-temperature calcination investigated by carbon inverse replication, Chem. Commun., (2001) 349–350.

[14] M. Kruk, M. Jaroniec, R. Ryoo, S.H. Joo, Characterization of ordered mesoporous carbons synthesized using mcm-48 silicas as templates, J. Phys. Chem. B., 104 (2000) 7960–7968.

[15] P. Xu, G.M. Zeng, D.L. Huang, Use of iron oxide nanomaterials in wastewater treatment: a review, Sci. Total Environ., 424 (2012) 1–10.

[16] C.L. Warner, W. Chouyyok, K.E. Mackie, Manganese doping of magnetic iron oxide nanoparticles: tailoring surface reactivity for a regenerable heavy metal sorbent, Langmuir, 28 (2012) 3931–3937.

[17] A.E. Karatapanis, D.E. Petrakis, C.D. Stalikas, A layered magnetic iron/iron oxide nanoscavenger for the analytical enrichment of ng-L(-1) concentration levels of heavy metals from water, Anal. Chim. Acta., 726 (2012) 22–27.

[18] H. Yang, Z. Tian, J. Wang, S. Yang, A magnetic resonance imaging nanosensor for Hg (II) based on thymidine-functionalized supermagnetic iron oxide nanoparticles, Sens. Actuator B-chem., 161 (2012) 429–433.

[19] A.S. Teja, P.K. Koh, Synthesis, properties, and applications of magnetic iron oxide nanoparticles, Prog. Cryst. Growth Charact. Mater., 55 (2009) 22–45.

[20] E. Ahmad khan, S. Jahan, T. Alam Khan, Adsorption of methyl red on activated carbon derived from custard apple (*Annona squamosa*) fruit shell: Equilibrium isotherm and kinetic studies, J. Molec. Liq., 249 (2018) 1195–1211.

[21] T.A. Khan, E.A. Khan, S. Jahan, Adsorptive uptake of basic dyes from aqueous solution by novel brown linseed deoiled cake activated carbon: Equilibrium isotherms and dynamics, J. Environ. Chem. Eng., 4(3) (2016) 3084–3095.

[22] T.A. Khan, R. Rahman, E.A. Khan, Adsorption of malachite green and methyl orange onto waste tyre activated carbon using batch and fixed-bed techniques: isotherm and kinetics modeling, Model. Earth Syst. Environ., 3(1) (2017) 33–38.

[23] M.K. Sahu, U.K. Sahu, R.K. Patel, Correction: Adsorption of safranin-O dye on CO_2 neutralized activated red mud waste: process modelling, analysis and optimization using statistical design, RSC Adv., 6 (2016) 32721–32721.

[24] S. Zhang, X. Zhao, H. Niu, Y. Shi, Y. Cai, G. Jiang, Superparamagnetic Fe_3O_4 nanoparticles as catalysts for the catalytic oxidation of phenolic and aniline compounds, J. Hazard. Mater., 167 (2009) 560–566.

[25] A. Alizadeh, M.M. Khodaei, M. Beygzadeh, D. Kordestani, M. Feyzi, Biguanide-functionalized Fe_3O_4/SiO_2 magnetic nanoparticles: an efficient heterogeneous organosuper base catalyst for various organic transformations in aqueous media, Bull. Korean Chem. Soc., 33 (2012) 2546– 2552.

[26] M. Khabazipour, Sh. Shariati, F. Safa, SBA and KIT-6 mesoporous silica magnetite nanoparticles: Synthesis and characterization, Synth. React. Inorg. M., 46 (2016) 759–765.

[27] H. Hafizi, A.R. Najafichermahini, M. Saraji, G.H. Mohammadnezhad, The catalytic conversion of fructose into 5-hydroxymethylfurfural over acid-functionalized KIT-6, an ordered mesoporous silica, Chem. Eng. J., 294 (2016) 380–388.

[28] W. Dai, M. Zheng, Y. Zhao, S. Liao, G. Ji, J. Cao, Template synthesis of three-dimensional cubic ordered mesoporous carbon with tunable pore sizes, Nanoscale Res. Lett., 5 (2010) 103–107.

[29] Sh. Shariati, M. Golshekan, Optimization of cloud point extraction of copper with neocuproine from aqueous solutions using taguchi fractional factorial design, J. Anal. Chem., 69 (2014) 248–254.

[30] S.M.S. Danesh, H. Faghihian, Sh. Shariati, Sulfonic acid functionalized magnetite nanoporous-KIT-6 for removal of methyl green from aqueous solutions, J. Nano Res., 52 (2018) 54–70.

[31] Sh. Shariati, M. Faraji, Y. Yamini, A.A. Rajabi, Fe_3O_4 magnetic nanoparticles modified with sodium dodecyl sulfate for removal of safranin O dye from aqueous solutions, Desalination, 270 (2011) 160–165.

[32] R. Zeynolabedin, K. Mahanpoor, Preparation and characterization of nano-spherical $CoFe_2O_4$ supported on copper slag as a catalyst for photocatalytic degradation of 2-nitrophenol in water, J. Nanostruct. Chem., 7 (2017) 67–74.

[33] S. Rahnama, Sh. Shariati, F. Divsar, Synthesis of functionalized magnetite titanium dioxide nanocomposite for removal of Acid Fuchsine dye, Comb. Chem. High. T. Scr., 21 (2018) 583–593.

[34] H. Li, D. Xiao, H. He, R. Lin, P. Zuo, Adsorption behavior and adsorption mechanism of Cu(II) ions on amino-functionalized magnetic nanoparticles, Trans. Nonferrous Met. Soc. China, 23 (2013) 2657–2665.

[35] S.M.S. Danesh, H. Faghihian, Sh. Shariati, Sulfonic acid functionalized SBA-3 silica mesoporous magnetite nanocomposite for Safranin O dye removal, Silicon, (2018) DOI: 10.1007/s12633-018-9997-7.

[36] J.F. Gao, Q. Zhang, K. Su, R.N. Chen, Y.Z. Peng, Biosorption of Acid Yellow 17 from aqueous solution by non-living aerobic granular sludge, J. Hazard. Mater., 174 (2010) 215–225.

[37] M.B. Gholivand, Y. Yamini, M. Dayeni, S. Seidi, E. Tahmaseb, Adsorptive removal of alizarin red-S and alizarin yellow GG from aqueous solutions using polypyrrole-coated magnetic nanoparticles, J. Environ. Chem. Eng., 3 (2015) 529–540.

[38] I. Langmuir, The adsorption of gases on plane surfaces of glass, mica and platinum, J. Am. Chem., 40 (1918) 1361–1403.

[39] E. Bulut, M. Özacar, İ.A. Şengil, Equilibrium and kinetic data and process design for adsorption of congo red onto bentonite, J. Hazard. Mater., 154 (2008) 613–622.

[40] S. Senthilkumaar, P. Kalaamani, K. Porkodi, P.R. Varadarajan, C.V. Subburaam, Adsorption of dissolved Reactive red dye from aqueous phase onto activated carbon prepared from agricultural waste, Bioresour. Technol., 97 (2006) 1618–1625.

[41] M.M.A. El Latif, A.M. Ibrahim, M.S. Showman, R.R.A. Hamide, Int. J. Nonferous Metall., 2 (2013) 47–62.

[42] I. Langmuir, The constitution and fundamental properties of solids and liquids, Part I. Solids. J. Am. Chem. Soc., 38 (1916) 2221–2295.

[43] M.A.K.M. Hanafiah, W.S.W. Ngah, S.H. Zolkafly, L.C. Teong, Z.A.A. Majid, Acid blue 25 adsorption on base treated (shoreadasyphylla) sawdust: kinetic, isotherm, thermodynamic and spectroscopic analysis, J. Environ. Sci., 24 (2012) 261–268.

[44] H. Freundlich, Über die Adsorption in Lösungen, W. Engelmann., 1906.

[45] L. Fan, Y. Zhang, X. Li, C. Luo, F. Lu, H. Qiu, Removal of alizarin red from water environment using magnetic chitosan with alizarin red as imprinted molecules, Colloids Surf. B: Biointerfaces, 91 (2012) 250–257.

[46] M.I. Temkin, V. Pyzhev, Kinetics of ammonica synthesis on promoted iron catalyst, Acta Phys. Chim., USSR 12 (1940) 327–356.

[47] C. Aharoni, M. Ungarish, Kinetics of activated chemisorption. Part 2. Theoretical models, J. Chem. Soc. Faraday Trans., 73 (1977) 456–464.

[48] V. Chandane, V.K. Singh, Adsorption of safranin dye from aqueous solutions using a low-cost agro-waste material soybean hull, Desal. Water Treat., 57(9) (2016) 4122–4134.

[49] S. Kaur, S. Rani, R.K. Mahajan, M. Asif, V.K. Gupta, Synthesis and adsorption properties of mesoporous material for the removal of dye safranin: Kinetics, equilibrium, and thermodynamics, J. Ind. Eng. Chem., 22 (2015) 19–27.

[50] S. Preethi, A. Sivasamy, S. Sivanesan, V. Ramamurthi, G. Swaminathan, Removal of Safranin basic dye from aqueous solutions by adsorption onto corncob activated carbon, Ind. Eng. Chem. Res., 45(2006) 7627–7632.

[51] H. Chaudhuri, S. Dash, S. Ghorai, S. Pal, A. Sarkar, SBA-16: Application for the removal of neutral, cationic, and anionic dyes from aqueous medium, J. Environ. Chem. Eng., 4 (2016) 157–166.

[52] M.K. Sahu, R.K. Patel, Removal of Safranin-O dye from aqueous solution using modified red mud kinetic and equilibrium studies, RSC Adv., 5 (2015) 78491–78501.

[53] K.O. Adebowale, B.I. Olu-Owolabi, E.C. Chigbundu, Removal of Safranin-O from aqueous solution by adsorption onto kaolinite clay, J. Encapsul. Adsorp. Sci., 4 (2014) 89–104.

[54] M.K. Dwivedi,N. Jain, P. Sharma, C. Alawa, Adsorption of Safranin from wastewater using coal fly ash, J. App. Chem., 8 (2015) 27–35.

[55] V.K. Gupta, A. Mittal, R. Jain, M. Mathur, S. Sikarwar, Adsorption of Safranin-T from wastewater using waste materials-activated carbon and activated rice husks, J. Adv. Colloid Interface Sci., 303 (2006) 80–86.

[56] T.A. Khan, M. Nazir, E.A. Khan, U. Riaz, Multiwalled carbon nanotube-polyurethane (MWCNT/PU) composite adsorbent for safranin T and Pb(II) removal from aqueous solution: Batch and fixed-bed studies, J. Molec. Liq., 212 (2015) 467–479.